Low-velocity impact positioning on composite honeycomb panels using a DPL-R regression

Zhaoyu Zheng[1], Ye He[2], Junshan Wang[3], Yan Tang[4], Shenzhen Tian[5]
Nanjing Vocational Institute of Transport Technology, Nanjing, Jiangsu, 211188, China
[1]Corresponding author
E-mail: [1]*zheng_zhaoyu@njitt.edu.cn*, [2]*434744183@qq.com*, [3]*wjsnuaa@163.com*, [4]*tangyan4job@foxmail.com*, [5]*1509431656@qq.com*

Received 31 December 2025; accepted 3 February 2026; published online 8 June 2026
DOI https://doi.org/10.21595/vp.2026.25959

76th International Conference on Vibroengineering in Tashkent, Uzbekistan, April 28-29, 2026

Abstract. This paper proposes a low-velocity impact localization method for carbon fiber/aluminum honeycomb panels using a regression framework based on Discriminative Projective Dictionary Pair Learning (DPL-R). Multi-channel FBG responses are converted into statistical features and mapped through a discriminative dictionary pair to obtain sparse representations, which are used for coordinate regression with a residual-weighted strategy. The method requires no wave-velocity modeling or finite-element simulation, making it suitable for complex panels under low sampling rates. Experiments on a 14×14 training grid and 20 free impacts show an average error of 3.64 mm, demonstrating its effectiveness for satellite-borne composite panel monitoring.

Keywords: composite materials, sparse representation, impact localization, SHM.

1. Introduction

Composite structures are widely used in spacecraft but are vulnerable to low-velocity impacts (LVI) that cause barely visible yet critical damage, making rapid impact localization essential for structural health monitoring. Although FBG sensors are suitable for this task, traditional TOA/TDOA-based Lamb-wave localization requires high sampling rates and spatially uniform wave-speed models, which are difficult to satisfy in carbon fiber-aluminum honeycomb panels due to strong wave-speed variability and limited interrogator sampling rates (1 kHz). Finite-element-based approaches are computationally expensive. Therefore, a data-driven localization method that does not rely on wave-speed modeling is highly desirable [1-4].

To overcome these limitations, we propose a DPL-R–based localization approach that extracts statistical and structural features from multi-channel FBG responses, learns discriminative sparse representations, and predicts impact coordinates via a residual-weighted regression model. The method requires no wave-velocity estimation or finite-element simulation.

Experiments on a 30 mm × 30 mm honeycomb panel using a 14×14 training grid and 20 free impacts yield a mean error of 3.64 mm, outperforming existing methods and demonstrating strong potential for on-orbit SHM.

2. Methodology

2.1. Impact localization method design

A DPL-R-based were approached for LVI localization that transforms multi-channel FBG signals into discriminative sparse features and predicts impact coordinates via residual-weighted regression.

As shown in Fig. 1, the framework consists of a training and a testing stage. In training, the panel is discretized into a grid, controlled impacts are applied, FBG signals are preprocessed into features, and the DPL algorithm learns a discriminative dictionary pair. In testing, features from

an unknown impact are projected into the learned subspace to obtain sparse coefficients. Reconstruction residuals for candidate locations are computed, and a weighted centroid based on inverse residuals yields the final impact coordinate.

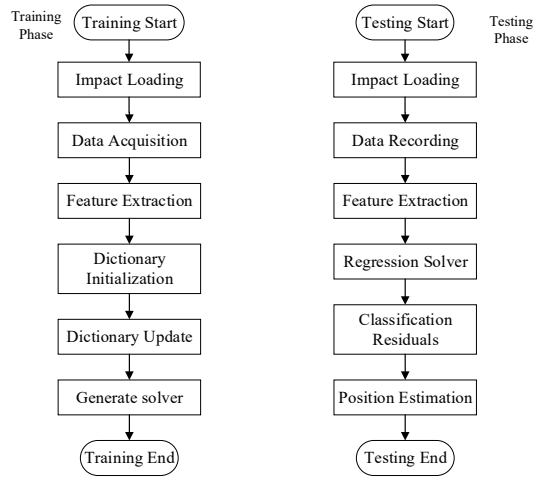

Fig. 1. Flowchart of the proposed localization approach

2.2. Principle of the method

2.2.1. FBG sensing principle

An FBG reflects a wavelength shift under strain satisfies [5-6]:

$$\frac{\Delta\lambda_B}{\lambda_B} = \{1 - P_e\}\varepsilon. \tag{1}$$

When an FBG sensor is attached to the surface of the composite panel and a low-velocity impact is applied on the opposite side of the bonding location, the sensor records the corresponding Lamb-wave response waveform.

2.2.2. DPL regression sparse dictionary model

Sparse representation assumes signals can be reconstructed using a few basis atoms, enabling class-discriminative representations when an appropriate dictionary is learned [7-8]:

$$J_{(D,X)} = \arg\min_{(D,X)}\{\|Y - DX\|_F^2 + \lambda\|X\|_p + f(X,D)\}. \tag{2}$$

In the DPL scheme, a supplementary analysis dictionary is employed $P \in R^{mk\times p}$ is included to allow the coefficients to be computed directly through a linear projection mapping:

$$\{P^*, D^*\} = \arg\min_{P,D}\{\|Y - DPY\|_F^2 + \Psi(D,P,X)\}. \tag{3}$$

Thus, for a test input, the reconstruction error corresponding to its actual class meets the following condition:

$$identity(y_i) = \arg\min_i \|y - D_i P_i y\|_2. \tag{4}$$

To achieve continuous impact localization instead of discrete class labels, this work extends

DPL into a sparse-representation regression framework (DPL-R). Owing to the analysis-synthesis dictionary pair in DPL, sparse coefficients can be computed through direct linear projection without iterative ℓ1-norm optimization, resulting in high computational efficiency for both training and testing [9-10].

2.2.3. Centroid-based regression model using the DPL-R dictionary

The trained analysis dictionary P generates the sparse feature vector: $x = Py$. Impact coordinates are first predicted through linear regression:

$$\hat{t} = W(Py) + b, \quad \hat{t} = [\hat{X}, \hat{Y}]^T. \tag{5}$$

To obtain continuous and smoother localization, a residual-weighted centroid refinement is introduced:

$$\hat{x} = \frac{\sum_{i=1}^{K} \omega_i x_i}{\sum_{i=1}^{K} \omega_i}, \quad \hat{y} = \frac{\sum_{i=1}^{K} \omega_i y_i}{\sum_{i=1}^{K} \omega_i}, \quad \omega_i = \frac{1}{\|y - D_i P_i y\|_2^2 + \varepsilon}. \tag{6}$$

This combines sparse features, regression, and residual-based weighting to achieve high-resolution localization in continuous space.

3. Experiments and results

3.1. Experimental design

The specimen is a carbon-fiber/aluminum honeycomb sandwich panel (1-mm skins, 5-mm core) mounted in a single-edge-clamped configuration to emulate a small-satellite solar-array substrate. The measurement region on the front surface is divided into a 14×14 grid (196 labeled points). Impacts are applied on the front face, and FBG sensors bonded to the backside record the corresponding Lamb-wave responses.

Six FBGs are installed: five for impact sensing and one for temperature compensation. Their layout and positions are shown in Fig. 2(a). A pendulum with a 10-g spherical head delivers low-velocity impacts; a 60° release angle corresponds to an energy of 0.0189 J. The SM130 interrogator captures Bragg-wavelength shifts at 1 kHz.

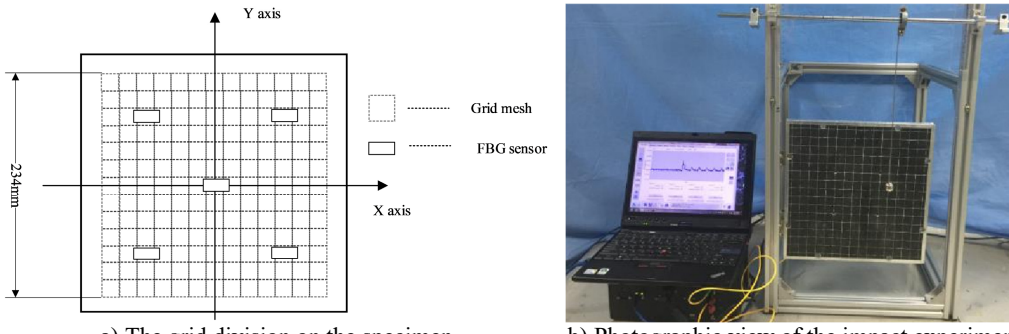

a) The grid division on the specimen b) Photographic view of the impact experiment

Fig. 2. Experimental setup for low-velocity impact tests. Photo taken by Zhaoyu Zheng in 2021 at the State Key Laboratory of Structural and Mechanical Engineering, Nanjing University of Aeronautics and Astronautics

Impact loads are generated using a pendulum mounted on an aluminum-frame fixture. A 10-g spherical impact head attached to a 350-mm rod produces low-velocity impacts; a 60° release angle corresponds to 0.0189 J. During impact, the induced stress waves propagate through the

sandwich panel and are captured by five FBG sensors using an SM130 interrogator at 1 kHz (Fig. 2(b)).

Each of the 196 grid points is impacted five times to create the training dataset, while twenty additional impacts at random, non-grid locations form the test set for evaluating generalization performance.

3.2. Feature extraction and parameter selection

Time-domain signals from five FBG channels are used for feature construction. Because the 1 kHz sampling rate limits accurate arrival-time extraction, the method focuses on waveform-level descriptors, including energy, mean, variance, skewness, kurtosis, crest factor, impulse factor, and shape factor. The feature set employed in this work consists of the following components (Table 1).

Table 1. Feature set used for impact signal characterization

Feature	Mathematical definition	Feature	Mathematical definition
Energy (E)	$E = \sum y\,(t)^2$	Kurtosis	$\frac{1}{N}\sum\left(\frac{y(t)-\mu}{\sigma}\right)^4$
Mean (μ)	$\mu = \frac{1}{N}\sum y\,(t)$	Crest factor (CF)	$CF = \frac{\max_t \lvert y(t)\rvert}{\sqrt{\frac{1}{N}\sum_{t=1}^{N} y\,(t)^2}}$
Variance (σ)	$\sigma = \sqrt{\frac{1}{N}\sum (y(t)-\mu)^2}$	Impulse factor (IF)	$IF = \frac{\max_t \lvert y(t)\rvert}{\frac{1}{N}\sum_{t=1}^{N} \lvert y(t)\rvert}$
Skewness	$\frac{1}{N}\sum\left(\frac{y(t)-\mu}{\sigma}\right)^3$	Shape factor (SF)	$SF = \frac{\sqrt{\frac{1}{N}\sum_{t=1}^{N} y\,(t)^2}}{\frac{1}{N}\sum_{t=1}^{N} \lvert y(t)\rvert}$

These features represent the envelope and morphology of each response waveform. To improve robustness against varying impact intensities, inter-channel structural information is also incorporated. For each channel pair (i, j) the correlation coefficient.

Each impact sample therefore yields a compact 50-dimensional feature vector that captures both single-channel temporal characteristics and inter-sensor relationships, and this vector is used as the input for DPL-R training and testing.

The DPL framework involves three parameters: λ, τ, and m. Here, m denotes the number of training samples used to construct the dictionary atoms, which was set to $m = 5$ in the experiments. The regularization parameters λ, τ were selected via six-fold cross-validation on the training data to ensure stable performance and avoid overfitting.

3.3. Results and analysis

In addition to the proposed DPL-R-based regression model (experimental group), three control groups were established for comparison:

(1) A support vector regression (SVR) model [11].

(2) A regression model based on the Fisher Discrimination Dictionary Learning (FDDL-R) [9].

(3) A DPL classifier without a regression module (DPL), which outputs only discrete class labels corresponding to the predefined grid points.

The impact localization results of all methods are shown in Fig. 3.

The results unmistakably show that the DPL-R approach achieves the highest localization accuracy among all evaluated methods. The average localization error of DPL-R is 3.64 mm, significantly lower than those of FDDL-R (4.95 mm) and SVR (5.35 mm). Due to its classification-only nature, the DPL method assigns each test sample to the nearest grid class,

resulting in the largest average error of 7.48 mm.

The observed error distribution indicates that central impact events are localized with greater precision. This behavior can be attributed to the strong attenuation of Lamb waves during transmission through the honeycomb core. For impacts near the center, all five FBG sensors receive relatively strong responses, enabling better extraction of discriminative multi-channel features. However, when the impact occurs near the boundary, one or more sensors record significantly weaker signals, degrading the waveform's inherent structural and shape-related characteristics, which reduces the ability of the learned features to distinguish between different impact locations.

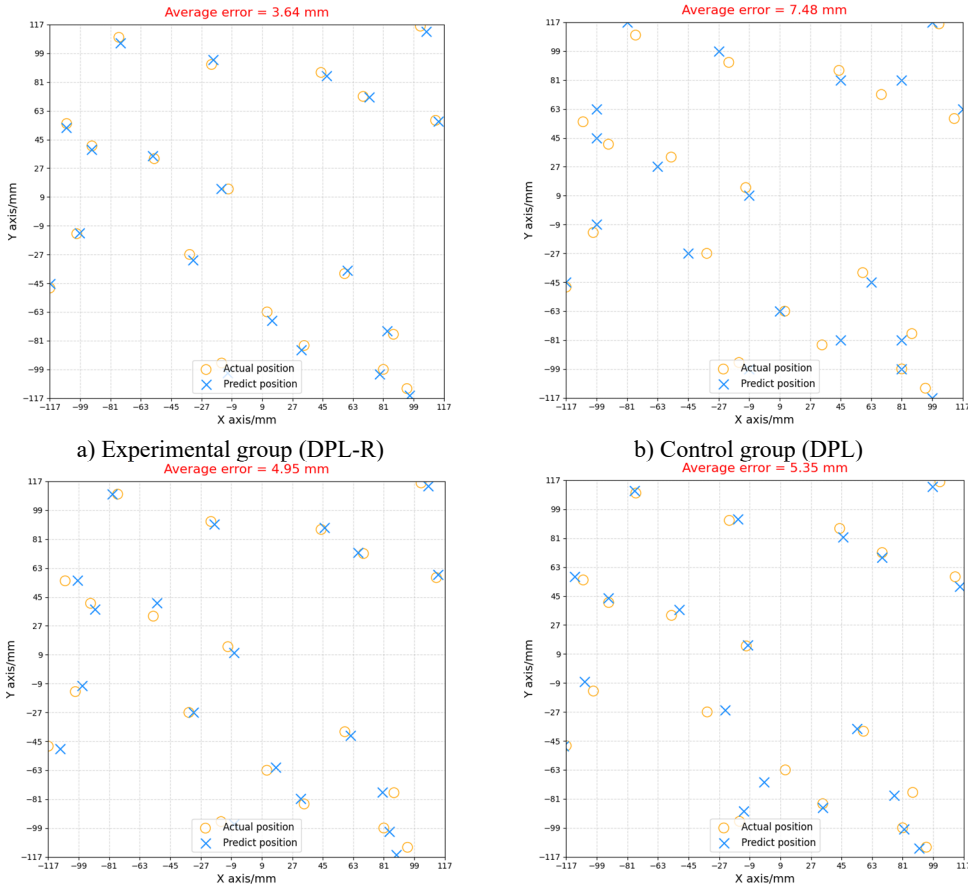

a) Experimental group (DPL-R) b) Control group (DPL)

c) Control group (FDDL-R) d) Control group (FDDL-R)

Fig. 3. The localization result of experimental group and control group

4. Conclusions

This study presents a DPL-R-based sparse representation regression method for low-velocity impact localization in carbon-fiber/aluminum honeycomb structures. Multi-channel FBG responses are transformed into statistical and structural features, and a discriminative dictionary pair is learned to obtain separable sparse representations. Combined with linear regression and a residual-weighted centroid strategy, the method predicts impact coordinates in continuous space without relying on wave-speed models or finite-element simulation.

Experiments show an average localization error of 3.64 mm, outperforming DPL, FDDL-R, and SVR. Accuracy is highest near the panel center and decreases toward the edges due to signal

attenuation. These results demonstrate the effectiveness and robustness of sparse-representation-based learning under low sampling rates and complex structural conditions, highlighting its suitability for lightweight composite panels in small satellites. Future work will explore multi-energy impact identification, real-time implementation, and system integration.

Acknowledgements

This work was supported by the Research Startup Funding for High-Level Talent (Grant No. JG2527), the Scientific Research Program in Natural Science (Grant No. JZ2405) at Nanjing Vocational Institute of Transport Technology, and the Natural Science Foundation of the Higher Education Institutions of Jiangsu Province, China (Grant No. 23KJB460020).

Data availability

The datasets generated during and/or analyzed during the current study are available from the corresponding author on reasonable request.

Conflict of interest

The authors declare that they have no conflict of interest.

References

[1] A. Ramezani, M. R. Esfahani, and J. Sabzi, "Strengthening of reinforced concrete beams using fiber-reinforced cementitious matrix systems fabricated with custom-designed mortar and fabrics," *Frontiers of Structural and Civil Engineering*, Vol. 17, No. 7, pp. 1100–1116, Sep. 2023, https://doi.org/10.1007/s11709-023-0967-9

[2] T. Liu, Y. Gao, X. Wang, S. Cheng, R. Zhu, and Y. Chen, "Design, manufacturing, and compressive properties of three-dimensional woven honeycomb composites," *Polymer Composites*, Vol. 46, No. 10, pp. 9646–9658, Jul. 2025, https://doi.org/10.1002/pc.29584

[3] K.-W. Kang, H. S. Kim, M. S. Kim, and J.-K. Kim, "Strength reduction behavior of honeycomb sandwich structure subjected to low-velocity impact," *Materials Science and Engineering: A*, Vol. 483-484, pp. 333–335, Jun. 2008, https://doi.org/10.1016/j.msea.2006.08.150

[4] Y. Karsandik, B. Sabuncuoglu, B. Yildirim, and V. V. Silberschmidt, "Impact behavior of sandwich composites for aviation applications: A review," *Composite Structures*, Vol. 314, p. 116941, Jun. 2023, https://doi.org/10.1016/j.compstruct.2023.116941

[5] K. O. Hill and G. Meltz, "Fiber Bragg grating technology fundamentals and overview," *Journal of Lightwave Technology*, Vol. 15, No. 8, pp. 1263–1276, Jan. 1997, https://doi.org/10.1109/50.618320

[6] W. H. Kim et al., "Recent progress in chalcogenide fiber technology at NRL," *Journal of Non-Crystalline Solids*, Vol. 431, pp. 8–15, Jan. 2016, https://doi.org/10.1016/j.jnoncrysol.2015.03.028

[7] D. L. Donoho and M. Elad, "Optimally sparse representation in general (nonorthogonal) dictionaries via ℓ 1 minimization," *Proceedings of the National Academy of Sciences*, Vol. 100, No. 5, pp. 2197–2202, Mar. 2003, https://doi.org/10.1073/pnas.0437847100

[8] J. Wright, A. Ganesh, Zihan Zhou, A. Wagner, and Yi Ma, "Demo: Robust face recognition via sparse representation," in *Gesture Recognition (FG)*, Sep. 2008, https://doi.org/10.1109/afgr.2008.4813404

[9] M. Yang, L. Zhang, X. Feng, and D. Zhang, "Sparse representation based fisher discrimination dictionary learning for image classification," *International Journal of Computer Vision*, Vol. 109, No. 3, pp. 209–232, May 2014, https://doi.org/10.1007/s11263-014-0722-8

[10] S. Gu, L. Zhang, W. Zou, and X. Feng, "Projective dictionary pair learning for pattern classification," in *Advances in Neural Information Processing Systems*, 2014.

[11] P. Liang, F. Duan, J. Wang, and H. Zhou, "Localization method for rock acoustic emission sources based on single sensor data and SVR-GBR machine learning models," *Measurement*, Vol. 245, p. 116566, Mar. 2025, https://doi.org/10.1016/j.measurement.2024.116566